Neutral pion cross section and spin asymmetries at forward rapidity in polarized proton collisions at $\sqrt{s} = 200$ GeV.

Insert Author List

(Dated: April 1, 2013)

The differential cross section and spin asymmetries for neutral pion production with pseudorapidity $0.8 < \eta < 2.0$ in polarized proton-proton collisions at $\sqrt{s} = 200$ GeV are presented. Data were taken using the endcap electromagnetic calorimeter in the STAR detector at RHIC. The cross section was measured over a transverse momentum range of $5 < p_T < 16$ GeV/c and is found to be within the scale uncertainty of a next-to-leading order perturbative QCD calculation. The longitudinal double-spin asymmetry, A_{LL}, is sensitive to the gluonic contribution to the proton spin, ΔG, and probes a lower Bjorken-x range than mid-rapidity measurements. The measured A_{LL} is consistent with model predictions. The transverse spin asymmetry, A_N spans a previously unmeasured kinematic range in x_F and p_T, and may help distinguish between contributions to A_N from the Sivers and Collins effects. The A_N results presented are consistent with zero. The parity violating asymmetry A_L is also measured and found to be consistent with zero.

PACS numbers: *insert PACS*

I. INTRODUCTION

The production of π^0-mesons in $\vec{p} + \vec{p}$ collisions at $\sqrt{s} = 200$ GeV allows access to both quark and gluon distributions within the proton, coupled with π^0 fragmentation functions. At intermediate pseudorapidity, $0.8 < \eta < 2$, the quark-gluon subprocess dominates over gluon-gluon and quark-quark subprocesses. Previously published data on inclusive π^0 production in polarized proton-proton scattering has been at either central pseudorapidities [1–4] or at large pseudorapidity [5, 6]. The measurements described in this paper, taken at intermediate pseudorapidity, cover previously unmeasured regions of the x and Feynman-x, transverse momentum (x_F, p_T) kinematic domains.

The measured cross section can be compared with perturbative QCD (pQCD) calculations and add information regarding the gluon to π^0 fragmentation function. Previous cross section measurements at nearby kinematics [1, 7, 8] are typically within the pQCD prediction scale uncertainty, lying at about 0.6 to 0.8 of the central scale prediction in the region of $5 < p_T < 12$ GeV/c.

The double longitudinal spin asymmetry is sensitive to the gluon polarization distribution $\Delta g(x)$ [9]. The single longitudinal spin asymmetries are parity violating and are thus expected to be zero. While $\Delta g(x)$ in the range $0.05 < x < 0.2$ is becoming more constrained [10], little is known for $x < 0.05$. As two protons are involved in the collision, there are two x values, with the larger x value is being denoted x_1 and the smaller x_2. In quark-gluon scattering, x_1 is associated with the quark and x_2 with the gluon. The production of π^0-mesons with $0.8 < \eta < 2.0$ covers approximately the range $0.1 < x_1 < 0.5$ and $0.01 < x_2 < 0.33$, with x_1 and x_2 increasing with increasing p_T. Fig. 1 shows Bjorken x_1 and x_2 distributions for two representative p_T bins, based on a Pythia [11] simulation.

The single transverse spin asymmetry for $x_F > 0$ has several possible contributions, including the Sivers and Collins effects at twist-2 [12], as well as higher twist effects [13]. Various measurements at different kinematic regions are needed to distinguish between these contributions. The A_N measurements described in this paper cover the previously unmeasured region $0.06 < x_F < 0.27$ and $5 < p_T < 12$ GeV/c.

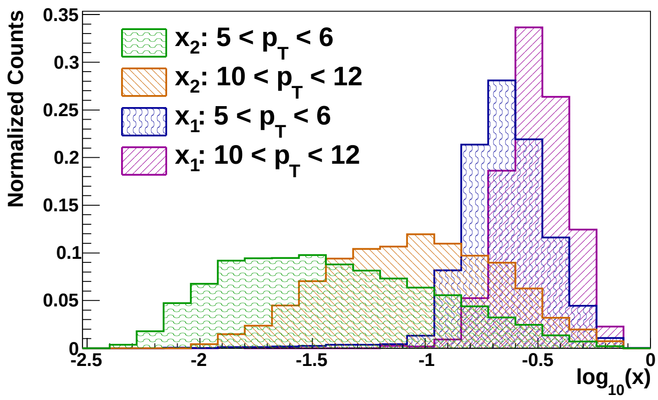

FIG. 1. Distribution of x_1 and x_2 in two different π^0 p_T bins.

II. ANALYSIS

The data used for these measurements were taken during the 2006 RHIC run. The data for the cross section were extracted from a sampled luminosity of 8.0 pb^{-1}, while the data for the longitudinal and transverse asymmetries were extracted from sampled luminosities of 4.8 pb^{-1} and 2.8 pb^{-1}, respectively. The data were taken with the STAR detector [14] at RHIC. The vertex positions are determined using charged particle tracks in the time projection chamber (TPC) [15]. The beam-beam counters (BBCs) are used to determine luminosity and contribute to the event trigger.

The endcap electromagnetic calorimeter (EEMC) is used to measure the energy deposition and position of photons from π^0 decays. The EEMC is a lead-scintillator sampling calorimeter [16], with the first two layers and last layer being read out independently as preshower and postshower layers. Each layer in the EEMC consists of 720 independent segments formed from 12 steps in pseudorapidity (η) and 60 steps in azimuth (ϕ). The segments in all layers corresponding to a specific (η,ϕ) range, when taken together, are called a "tower". A shower maximum detector (SMD) is located between layers five and six, consisting of two layers of tightly packed 1 cm wide scintillating strips.

Photons are reconstructed by first clustering the energy depositions in the SMD strips to determine the position in η, ϕ, and then using the EEMC towers to measure the photon-energy. The EEMC towers are calibrated using the most probable value of Landau-peak for minimum ionizing particles. Only SMD energy clusters with at least 3 MeV of deposited energy and at least 2 MeV deposited in the central strip, are used for this analysis. Photons are further required to have energy of at least 2.0 GeV as measured in the associated tower(s) and to be within the fiducial volume of $1.11 < \eta_{det} < 1.96$, where η_{det} is the detector η, relative to the nominal interaction point. The physical η, determined relative to the TPC-reconstructed primary vertex, is required to be $0.8 < \eta < 2.0$. Further event selection requirements include: (a) coming from a valid bunch crossing, (b) the TPC-reconstructed vertex being within ± 120 cm of the nominal interaction point, (c) the π^0 candidate transverse momentum $p_T > 5$ GeV/c, and (d) the preshower energy being less than 40 MeV. All possible pairs of photons that satisfy these requirements are considered as π^0 candidates.

The limited number of photon statistics in each SMD strip can cause a cluster of energy deposited by a single photon to appear as two clusters of energy, thus causing two reconstructed photons. This "false splitting" effect accounts for a large fraction of π^0 candidates with invariant mass below 0.1 GeV/c^2. False splitting can be somewhat mitigated by a "merging" procedure. If two π^0 candidates are found within $\sqrt{\Delta\eta^2 + \Delta\phi^2} < 0.05$ then these candidates are replaced with a new, merged candidate. The momentum of the merged candidate is set to the sum of the momentum of the contributing photons, without double counting photons that were included in the original π^0 candidates. This merging step has negligible effect on the π^0 reconstruction efficiency. The other large contributor to low mass π^0 candidates is the case in which a real π^0s has one of the SMD clusters is not reconstructed. The cluster may have been lost due to being below the energy threshold, yet it appears as the more frequent case of two clusters having no separation in the direction of one of the layers. The real π^0 with the lost cluster will have its opening angle, and thus its mass, reconstructed lower than the true value.

All events considered in this analysis are from a single trigger that includes a coincidence requirement in the two BBCs, implying a $p+p$ collision. The trigger requires at least one tower with transverse energy above a given threshold and with the total transverse energy in the 3×3 "patch" of towers surrounding and including the high energy tower to be above a second threshold. Although hardware thresholds varied over the course of the data taking, the analysis included an emulated trigger requirement, with thresholds of 4.326 GeV and 6.18 GeV, respectively, for the high energy tower and the 3x3 tower patch. These emulated trigger thresholds were 10% above the maximum hardware triggers.

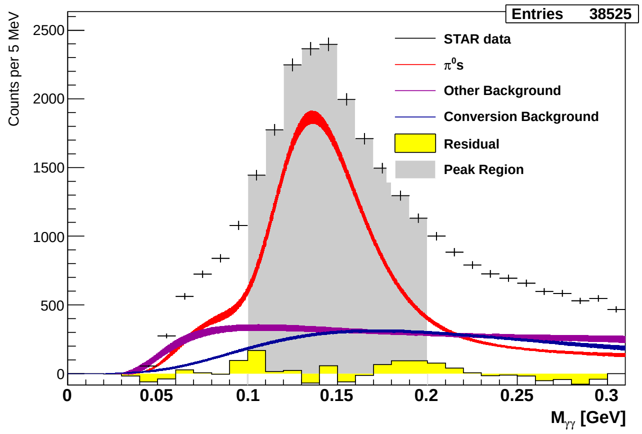

FIG. 2. Invariant mass distribution for the two-photon system with $8 < p_T < 9$ GeV/c. Also included on the plot are the template functions for the signal and two backgrounds (scaled and shifted according to the fit results), the residual between the data and the sum of the templates, and a gray-shaded area indicating the signal region.

The signal fraction was determined by fitting a linear combination of template functions to the two-photon invariant mass ($M_{\gamma\gamma}$) distribution over the range $0.0 < M_{\gamma\gamma} < 0.3$ GeV/c^2 for each p_T (or x_F) bin. Three template functions were determined by fitting the functions to Pythia Monte Carlo data to represent (a) the π^0 signal, (b) the conversion background where the two reconstructed "photons" that formed the π^0 candidate were actually the two leptons from a photon that converted in material upstream of the EEMC, and (c) all other backgrounds, including combinatoric backgrounds. When fitting the weights of the three template functions an additional factor was also included to account for the energy scale difference between the data and the Monte Carlo. This energy scale difference was not simply related to the calibration, but was also affected by assumptions about the signal fraction used in the simulation.

The data and template functions for the $8 < p_T < 9$ GeV/c bin are shown in Fig. 2. While the fits to determine the signal fraction cover $0 < M_{\gamma\gamma} < 0.3$, only π^0 candidates with $M_{\gamma\gamma}$ in the range $0.1 < M_{\gamma\gamma} < 0.2$ GeV/c^2 (defined as the peak region) were used for the remainder of the analysis. The signal fraction in the peak region was computed from the weights, the data vs. simulation energy scale factor, and integrals of the template functions. The product of the signal fraction in the peak region and the number of π^0 counts within this region then gives the number of background-subtracted π^0s for the given bin.

To compute the cross section, the number of background-subtracted π^0s was corrected for p_T bin smearing by applying the inverse of a smearing matrix, obtained from the same Pythia Monte Carlo data set as used above. The final cross section was then computed using Eq. 1,

$$\frac{1}{E}\frac{d\sigma}{d\boldsymbol{p}^3} = \frac{1}{\Delta\phi\ \Delta\eta\ \Delta p_T}\frac{1}{\langle p_T\rangle}\frac{1}{\mathrm{BR}}\frac{1}{\epsilon}\frac{N}{\mathcal{L}}, \tag{1}$$

where N is the corrected number of π^0s, $\mathcal{L}$ is the sampled luminosity (including dead-time corrections), ϵ is the product of reconstruction and trigger efficiencies, BR is the branching ratio $\pi^0 \to \gamma\gamma$ [17], $\langle p_T\rangle$ is the average p_T for the particular p_T bin, Δp_T is the width of the p_T bin, and $\Delta\phi$ (equal to 2π) and $\Delta\eta$ (equal to 1.2) are the ϕ and η phase space factors. The trigger efficiency is below 10% for π^0s with $5 < p_T < 6$ GeV, and plateaus above 40% at $p_T \approx 9$ GeV/c. The reconstruction efficiency is around 30% for $5 < p_T < 9$ GeV/c, and decreases to around 20% for $12 < p_T < 16$ GeV/c.

The longitudinal spin asymmetries were computed by subtracting the luminosity asymmetry from the asymmetry in the number of π^0 candidates and dividing this difference by the luminosity-weighted polarization. Specifically,

$$\begin{aligned} A_{L,B} = \frac{1}{\langle P_B\rangle}\Bigg(&\frac{N^{++}+N^{+-}-N^{-+}-N^{--}}{N^{++}+N^{+-}+N^{-+}+N^{--}} \\ &-\frac{L^{++}+L^{+-}-L^{-+}-L^{--}}{L^{++}+L^{+-}+L^{-+}+L^{--}}\Bigg), \end{aligned} \tag{2}$$

$$\begin{aligned} A_{L,Y} = \frac{1}{\langle P_Y\rangle}\Bigg(&\frac{N^{++}-N^{+-}+N^{-+}-N^{--}}{N^{++}+N^{+-}+N^{-+}+N^{--}} \\ &-\frac{L^{++}-L^{+-}+L^{-+}-L^{--}}{L^{++}+L^{+-}+L^{-+}+L^{--}}\Bigg), \end{aligned} \tag{3}$$

$$\begin{aligned} A_{LL} = \frac{1}{\langle P_B P_Y\rangle}\Bigg(&\frac{N^{++}-N^{+-}-N^{-+}+N^{--}}{N^{++}+N^{+-}+N^{-+}+N^{--}} \\ &-\frac{L^{++}-L^{+-}-L^{-+}+L^{--}}{L^{++}+L^{+-}+L^{-+}+L^{--}}\Bigg), \end{aligned} \tag{4}$$

where subscripts represent the blue (momentum from the interaction region towards the EEMC) and yellow (momentum aimed away from the EEMC) beams, N is the number of counts in the signal region, L is the luminosity, and where the superscripts of B and Y designate the blue beam and yellow beams, respectively. The luminosity-weighted average polarizations have values $\langle P_B\rangle = 0.56$ and $\langle P_Y\rangle = 0.59$, and the luminosity-weighted average product of the polarizations has the value $\langle P_B P_Y\rangle = 0.33$.

The signal fraction was determined using data summed over the spin states. The asymmetries were corrected for the background asymmetry using Eq. 5,

$$A^{sig} = \frac{1}{s}\left(A^{raw} - (1-s)A^{bkg}\right), \tag{5}$$

where s is the signal fraction, A^{sig} is the asymmetry of the π^0 signal, A^{raw} is the asymmetry value before background subtraction (Eqs. 2, 3, and 4), and A^{bkg} is an estimate of the background asymmetry. The background asymmetries were estimated as the average of the asymmetry in the two sideband regions, and were found to be less than 1σ from zero, with $\sigma \approx 0.01$.

The transverse spin asymmetry was computed by binning with respect to ϕ, the angle between the azimuthal angles of the π^0 and the spin polarization vector. The raw cross ratio $\mathcal{E}(\phi)$ was computed per ϕ bin,

$$\mathcal{E}(\phi) = \frac{\sqrt{N^{\uparrow}(\phi)\,N^{\downarrow}(\phi+\pi)} - \sqrt{N^{\downarrow}(\phi)\,N^{\uparrow}(\phi+\pi)}}{\sqrt{N^{\uparrow}(\phi)\,N^{\downarrow}(\phi+\pi)} + \sqrt{N^{\downarrow}(\phi)\,N^{\uparrow}(\phi+\pi)}}, \tag{6}$$

where N represents the number of counts, $\uparrow$ denotes beam spin polarized in the positive-vertical direction relative to the beam momentum ("up"), and $\downarrow$ denotes beam spin polarized in the negative-vertical direction relative to the beam momentum ("down"). The quantity $\mathcal{E}_N(\phi)$ was fit to the equation $C + \varepsilon\sin\phi$, the background was subtracted using Eq. 5 with $A^{raw} = \varepsilon$, and the final result for A_N was obtained by dividing by the luminosity weighted polarization. The background asymmetries were estimated as the average of the asymmetry in the two sideband regions, and were found to be less than 1σ from zero, again with $\sigma \approx 0.01$.

III. RESULTS

A. Cross Section

Figure 3 shows the cross section results of this analysis in comparison with previously published STAR results in other pseudorapidity and transverse-momentum regions. While the entire STAR detector has a broad range of coverage, this result lies in a previously unmeasured region. The results indicate that the cross section is fairly flat with respect to η at lower η and has significant η dependence at higher η, with the transition lying between $\eta = 2$ and $\eta = 3.68$.

Figure 4 includes the cross section along with a theory curved based on pQCD and global fits of distribution and fragmentation functions. The EEMC π^0 cross section data points are observed to lie between the p_T and $2p_T$ scale. This is qualitatively consistent with published mid-rapidity STAR [1] and PHENIX results at $\sqrt{s} = 200$ GeV and $\sqrt{s} = 500$ GeV [7, 8]: in each of these results, the cross section is lower than the p_T-scale theory curve in the region of $6 < p_T < 16$ GeV/c. Such a disagreement

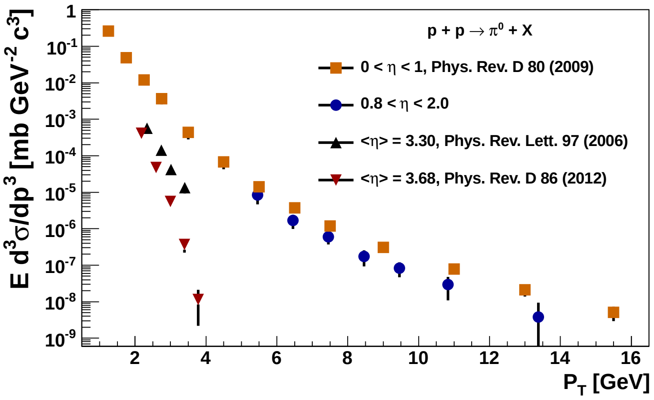

FIG. 3. The π^0 cross section at various pseudorapidities as measured by STAR. Error bars are total uncertainty. The ~~dark red square~~ the results of this analysis, while the other points are previously published results use the STAR barrel electromagnetic calorimeter (orange circles) [1] and the forward pion detectors (blue and black triangles) [5, 6].

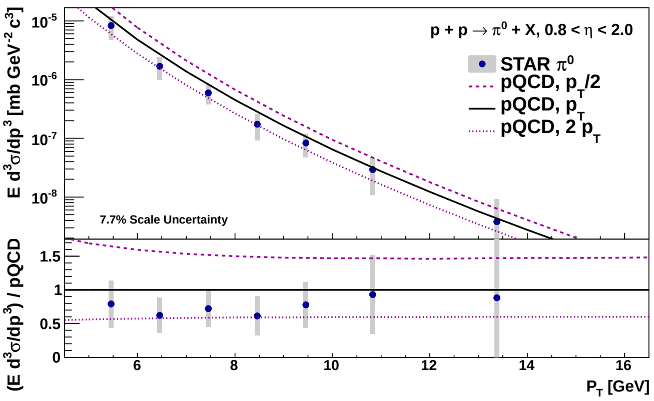

FIG. 4. Upper panel: the π^0 cross section (black markers) is shown compared with a pQCD calculation [18] with three options for the scale parameter. Statistical uncertainties are shown by the error bars, which is indistinguishable from the marker in most bins. Systematic uncertainties are shown by the error boxes. The lower panel presents the ratio of the data to the p_T-scale theory curve, as well as the ratio of the $2p_T$-scale and $p_T/2$-scale theory curves to the p_T-scale curve.

could indicate the importance of non-perturbative effects, or it may suggest the need for further refinements of the π^0 fragmentation function model.

Contributions to the systematic uncertainties include the uncertainty on the signal fraction, the uncertainty on the smearing matrix, the effect of repeating the analysis with an additional $4 < p_T < 5$ GeV/c bin, the uncertainty on the reconstruction and trigger efficiencies, and the EEMC energy resolution and overall EEMC energy scale. The signal fraction uncertainty includes contributions from the uncertainties of the parameters in the template functions, the uncertainty on the weights of the templates, the uncertainty on the scale parameter and its effect on the integrals used to determine the signal fraction in the peak, and a contribution based on the integral of the residual in the signal region. The dominant uncertainty on the cross section is the overall energy scale uncertainty, which is correlated over all bins.

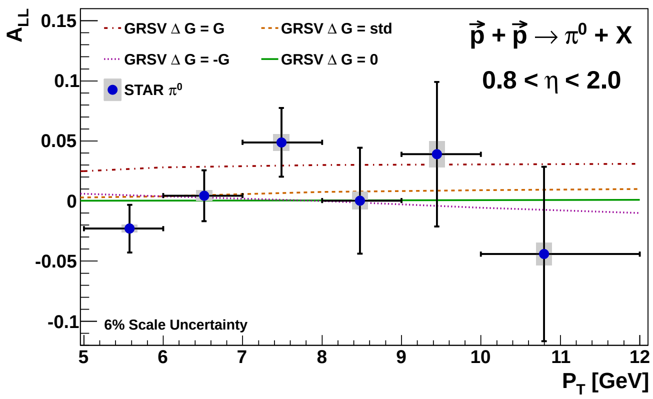

FIG. 5. The A_{LL} results (black markers) are presented with the GRSV prediction [19] using four different assumptions regarding ΔG. Statistical uncertainties are shown by the error bars, and systematic uncertainties are shown by the error boxes.

B. Longitudinal Asymmetries

The A_{LL} results for $5 < p_T < 12$ GeV/c are shown in Fig. 5. Systematic uncertainties include the uncertainty on the signal fraction and the uncertainty on the estimate of the background asymmetry. The relative luminosity uncertainty was found to be negligible compared to the statistical uncertainties. Fitting the results to a constant yields a value of $A_{LL} = 0.002 \pm 0.012$.

The A_{LL} results are consistent with the model predictions [19]. The model predictions are based on global fits of both deep inelastic scattering data and proton-proton collisions. Although the uncertainties of the results are somewhat large, the results correspond to lower Bjorken-x values than other published results and may thus have impact on the global extraction of $\Delta g(x)$. The procedures used in obtaining this result can also be applied to more recent data sets already recorded by STAR, which have higher luminosity and less material from the EEMC. The combined analysis of data from the same detector from multiple years will result in yet lower statistical uncertainties, the dominant uncertainty at present.

The two parity violating single spin asymmetries were also measured and are consistent with zero, as expected. The p_T integrated values, $5 < p_T < 12$, are -0.003 ± 0.007 (blue beam) and -0.001 ± 0.007 (yellow beam).

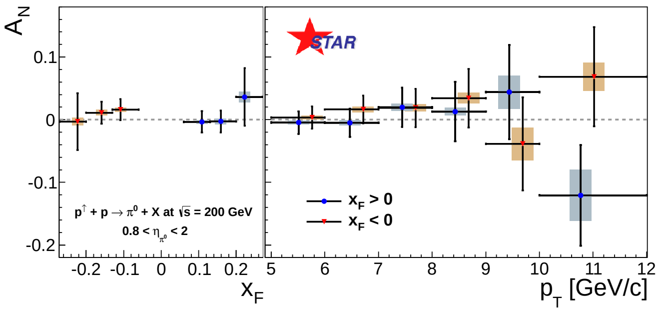

FIG. 6. The A_N results are plotted versus x_F (left panel) and versus p_T (right panel). Statistical uncertainties are shown by error bars, and systematic uncertainties are shown by error boxes. Negative x_F results are shown using red triangular markers and tan systematic error boxes, while positive x_F results are shown using blue circle markers and blue systematic error boxes.

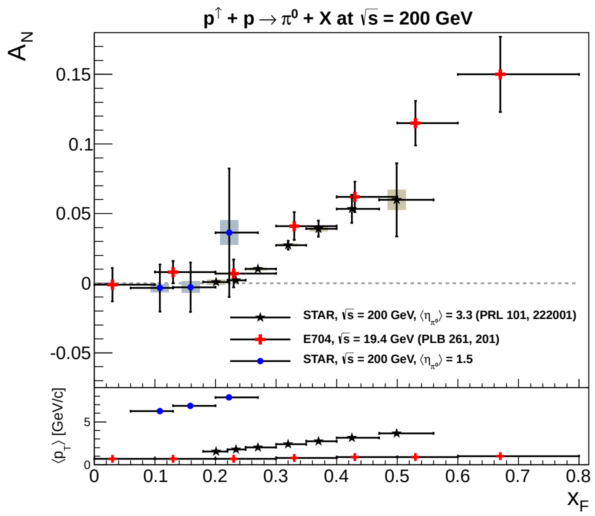

FIG. 7. Top panel: the A_N results for $x_F > 0$ versus x_F are compared with previously published values of A_N. Bottom panel: the average p_T value is shown for each x_F bin and for each experiment.

C. Transverse Spin Asymmetries

The A_N results versus x_F for $0.06 < x_F < 0.27$ and $5 < p_T < 12$ GeV/c are shown in the left panel of Fig. 6. Systematic uncertainties include the uncertainty on the signal fraction, the uncertainty on the estimate of the background asymmetry, and single beam backgrounds. The A_N results are compared with previously published results in Fig. 7. A_N is consistent with zero for $x_F < 0$, consistent with the prediction that this hadronic process is not parity violating. As anticipated from the previous results at lower p_T and similar x_F [3, 20, 21], A_N is also consistent with zero for $x_F > 0$. Fitting A_N to a constant results in $A_N = -0.001 \pm 0.012$ for $x_F > 0$ and $A_N = 0.012 \pm 0.012$ for $x_F < 0$, with $\langle |x_F| \rangle = 0.14$.

The A_N results versus p_T, over the same range of $0.06 < x_F < 0.27$ and $5 < p_T < 12$ GeV/c, are shown in the right panel of Fig. 6. At zero, A_N is expected to be zero [22], while at large p_T, A_N is expected to scale as $1/p_T$ [23]. At intermediate p_T, the behavior is unknown. Within the x_F region of this measurement, A_N is consistent with zero and no strong conclusions about the p_T dependence can be made.

IV. CONCLUSIONS

Neutral pions were detected in the STAR Endcap Electromagnetic Calorimeter, having been produced in polarized proton-proton collisions with $\sqrt{s} = 200$ GeV at RHIC. The production cross section, the double and single longitudinal spin asymmetries, and the single transverse spin asymmetry have been measured for π^0s with $0.8 < \eta < 2.0$ and with $5 < p_T < 12$ (spin asymmetries) or $5 < p_T < 16$ (cross section). These results sample a region of phase space not previously studied, complementing measurements in neighboring regions of this phase space. The cross section is slightly lower than previously published measurements at more central pseudorapidities and is within the scale uncertainty of a pQCD calculated prediction. The A_{LL} measurement is consistent with a model prediction and includes data with Bjorken x_2 reaching below 0.01. The measured values of the parity violating spin asymmetries, i.e. A_L and A_N for $x_F < 0$, are consistent with zero. The measured value of A_N for $x_F > 0$ is also consistent with zero, as anticipated from previous results at lower p_T.

[1] B. I. Abelev et al. (STAR), Phys. Rev. D p. 111108 (2009).
[2] (????), PHENIX ALL cross section.
[3] (????), E704 AN.
[4] (????), ATLAS pi0 xSec.
[5] (????), STAR FPD pi0 xSec 1.
[6] (????), STAR FPD pi0 xSec 2.
[7] A. Adare et al. (PHENIX), Phys. Rev. D p. 051106 (2007).
[8] (????), PHENIX pi0 cross section 500.
[9] (????), ALL theory paper.
[10] (????), latest delta G fit.

[11] S. M. T. Sjöstrand and P. Skands, p. 026 (2006).
[12] (????), AN Sivers and Collins.
[13] (????), AN higher twist effects.
[14] K. Aokermann et al. (STAR), Nucl. Inst. & Meth. **A499**, 624 (2003).
[15] M. Anderson et al., **499**, 659 (2003).
[16] C. Allgower et al., Nucl. Inst. & Meth. **A499**, 740 (2003).
[17] J. Beringer et al. (Particle Data Group), Phys. Rev. D p. 010001 (2012).
[18] (????), cross section theory curve.
[19] M. Glück et al., Phys. Rev. D **63**, 094005 (2001).
[20] (????), STAR FPD pi0 AN 1.
[21] (????), STAR FPD pi0 AN 2.
[22] (????), Theory paper discussing AN zero at pT = 0.
[23] (????), Theory paper discussing AN scaling at large pT.